HHS Public Access

Author manuscript

Neuroimage. Author manuscript; available in PMC 2021 October 20.

Published in final edited form as:

Neuroimage. 2021 October 15; 240: 118391. doi:10.1016/j.neuroimage.2021.118391.

Functional networks in non-human primate spinal cord and the effects of injury

Anirban Sengupta[a,c], **Arabinda Mishra**[a,c], **Feng Wang**[a,c], **Muwei Li**[a,c], **Pai-Feng Yang**[a,c], **Li Min Chen**[a,c,#,*], **John C. Gore**[a,b,c,d,#]

[a]Vanderbilt University Institute of Imaging Science, Nashville, TN, 37232, USA

[b]Biomedical Engineering, Vanderbilt University, Nashville, TN, 37232, USA

[c]Radiology and Radiological Sciences, Vanderbilt University Medical Center, Nashville, TN, 37232, USA

[d]Department of Physics and Astronomy, Vanderbilt University, Nashville, TN, 37232, USA

Abstract

Spontaneous fluctuations of Blood Oxygenation-Level Dependent (BOLD) MRI signal in a resting state have previously been detected and analyzed to describe intrinsic functional networks in the spinal cord of rodents, non-human primates and human subjects. In this study we combined high resolution imaging at high field with data-driven Independent Component Analysis (ICA) to i) delineate fine-scale functional networks within and between segments of the cervical spinal cord of monkeys, and also to ii) characterize the longitudinal effects of a unilateral dorsal column injury on these networks. Seven distinct functional hubs were revealed within each spinal segment, with new hubs detected at bilateral intermediate and gray commissure regions in addition to the bilateral dorsal and ventral horns previously reported. Pair-wise correlations revealed significantly stronger connections between hubs on the dominant hand side. Unilateral dorsal-column injuries disrupted predominantly inter-segmental rather than intra-segmental functional connectivities as

[*]Corresponding author. limin.chen@vanderbilt.edu (L.M. Chen).
[#]equally responsible for directing the study

Data and Code Sharing Statement

The authors confirm that the data and code supporting the findings of this study will be made available upon reasonable request to the corresponding author, Li Min Chen.

Materials & Correspondence

Any Data or code requests should be addressed to the corresponding author Dr. Li Min Chen.

Ethical Statement

All procedures followed NIH guidelines on the care and use of laboratory animals and were approved by IACUC (Institutional Animal Care and Use Committee) of Vanderbilt University.

Declaration of Competing Interest

None

Credit authorship contribution statement

Anirban Sengupta: Formal analysis, Investigation, Validation, Writing – original draft, Writing – review & editing. **Arabinda Mishra:** Formal analysis, Software, Methodology. **Feng Wang:** Data curation, Methodology. **Muwei Li:** Software. **Pai-Feng Yang:** Data curation, Methodology. **Li Min Chen:** Conceptualization, Supervision, Investigation, Writing – review & editing. **John C. Gore:** Conceptualization, Supervision, Investigation, Funding acquisition, Writing – review & editing.

Supplementary materials

Supplementary material associated with this article can be found, in the online version, at doi: 10.1016/j.neuroimage.2021.118391.

revealed by correlation strengths and graph-theory based community structures. The effects of injury on inter-segmental connectivity were evident along the length of the cord both below and above the lesion region. Connectivity strengths recovered over time and there was revival of inter-segmental communities as animals recovered function. BOLD signals of frequency 0.01–0.033 Hz were found to be most affected by injury. The results in this study provide new insights into the intrinsic functional architecture of spinal cord and underscore the potential of functional connectivity measures to characterize changes in networks after an injury and during recovery.

Keywords

BOLD fMRI; Resting state functional connectivity; Spinal cord; Independent Component Analysis; Dorsal column injury; Graph Theory

1. Introduction

The spinal cord is responsible for the transmission and integration of signals to and from the brain, and acts as the primary interface between the central and peripheral nervous systems (Prochazka and Mushahwar, 2001). The cervical spinal cord is thought to contain neural circuits that are involved in skilled hand sensorimotor behavior (Harel et al., 2008; Isa, 2019; Sher et al., 2010) and the control of upper arms and hands. Movements such as skillful reaching and grasping are considered to be governed primarily by neural circuitries in supraspinal brain regions including the primary motor cortex (M1), which connects directly to motor neurons in the spinal cord ventral horn via the corticospinal pathway (CS) (Alstermark and Isa, 2012). However, recent findings from studies of normal animals and animals with complete and incomplete spinal cord injury (SCI) have challenged this long-standing view and suggest that circuits within spinal cord also play an essential role in integrating and possibly gating the descending CS signals, and mediate recovery of movements after spinal cord injury (SCI) (Rossignol and Frigon, 2011). In particular, ex vivo and behavioral studies have suggested that mid-level cervical segments (C3-C4) may serve as a modulating center for CS signals directed to the cervical enlargement segments (C5-C6-C7) and provide dynamic control of arm movement and skilled hand use (Alstermark and Isa, 2012). However, the organization and roles of such intra- and inter-segmental circuits remains largely unexplored. Using sub-millimeter resolution fMRI and tract-tracing histology, we recently confirmed the existence of intrinsic functional circuits in cervical spinal segments of nonhuman primates (Chen et al., 2015). We also found that disruptions of measures from chemical exchange saturation transfer (CEST) and quantitative magnetization transfer (qMT) within these networks using MRI, correlate with impairments in skilled hand reaching and grasping behavior in monkeys, and the time courses of recovery of typical CEST peak amplitude and pool size ratio (PSR) from qMT were associated with improvements in hand functions (Wang et al., 2018, 2019). The goal of the current study was to expand previous findings to increase our understanding of the functional organization of intrinsic circuits in the cervical spinal cord that are engaged in the control of skilled hand use, and to demonstrate their behavioral relevance by quantifying changes in networks after a targeted injury and during recovery.

Resting-state functional connectivity (rsFC) between regions can be obtained from measurements of the correlations between BOLD (blood oxygenation-level dependent) signals obtained using functional magnetic resonance imaging (fMRI). RsFC has been widely used to identify and characterize functional circuits in the brain, and also used to quantify changes in such circuits under different conditions (Ferreira and Busatto, 2013; Guerra-Carrillo et al., 2014; Van den Heuvel and Hulshoff Pol, 2010). However, there have been few reports of rsFC in the spinal cord partly because imaging of the spinal cord is challenging due to its smaller physical size, the impact of pronounced physiological noise, and detrimental effects from susceptibility gradients during imaging (Barry et al., 2018; Eippert et al., 2017b; Harrison et al., 2021). Our group was among the first to use MRI to demonstrate robust rsFC between the dorsal and ventral horns in both human and animal models (Barry et al., 2017; Chen et al., 2015; Wu et al., 2019). These studies illustrated that a characteristic, reproducible, intrinsic functional architecture was detectable within spinal cord gray matter (Barry et al., 2014; Kinany et al., 2020; Kong et al., 2014). However, to date rsFC data have been interpreted in terms of relatively simple models of connectivity incorporating only the four spinal horns. There is a need to extend such models in order to understand the complexities of intrinsic functional circuits of cervical spinal cord more fully. Here we report our findings of additional networks and connectivities in the spinal cord of non-human primates using high resolution and high field fMRI.

We have previously used seed-based correlation analysis (Chen et al., 2015; Wu et al., 2018; Barry et al., 2017) to quantify functional connectivity between spinal horns. Given the time series of MRI signal from a seed voxel or a region of interest (ROI), seed based connectivity is calculated as the Pearson correlation between this voxel and the corresponding time series of every other voxel. However, seed-based analyses are limited by *a priori* hypotheses about which regions are engaged in networks and, in previous studies of the spinal cord, that the four horns constitute the relevant functional hubs in gray matter (Barry et al., 2018, 2014; Chen et al., 2015). Alternative data driven approaches have the advantage of not requiring prior hypotheses about the components of functional circuits within any given structure. Such methods are well suited to uncover novel circuits that may not have previously been identified. Some previous studies have used Independent Component Analysis (ICA) as a data driven technique to identify functional circuits in the spinal cord (Kong et al., 2014; Nateras et al., 2016; Wei et al., 2010). Kong et al. (2014) performed ICA on spinal cord data but restricted their analysis to only dorsal and ventral horns (Kong et al., 2014). Nateras et al (2016) used ICA and detected a functional cluster within the central spinal cord (apart from the 4-horns) but did not investigate its connectivity with the dorsal and ventral horns. Both these studies were performed at 3 Tesla on human subjects, which may not give adequate spatial resolution or sensitivity to unravel finer details of spinal cord functional architecture within and between spinal segments. Also, they included the entire spinal cord (including both white and gray matter) in their spatial analyses, which possibly introduced influences from white matter signals in their results. Thus, further investigation is warranted to establish the spatial arrangements of independent functional hubs within the spinal cord beyond the ‘4 horn model’ using a data driven approach at a higher field strength and spatial resolution, considering only the butterfly-shaped gray matter in each segment as the relevant functional apparatus of spinal cord.

Injuries to the spinal cord may impair sensory, autonomic and/or motor functions, so methods for assessing the functional integrity of the spinal cord are directly relevant clinically. Disruptions of functional connectivity within the spinal cord may occur after traumatic injury or as a result of various musculoskeletal or neurodegenerative diseases (Chen et al., 2015; Conrad et al., 2018; Simpson et al., 2012; Stroman et al., 2016). It has also been found that thermal stimulation and physiological pain signaling can alter cervical spinal cord functional connectivity in humans (Sprenger et al., 2015; Weber et al., 2018). Here we report the effects of a targeted injury to the dorsal column of monkey spinal cord on intrinsic resting state networks to demonstrate their functional relevance and potential value as indicators of spinal cord injury and recovery. The effects of injury and of interventions are mainly assessed using behavioral outcomes in both preclinical animal and clinical human studies (Goldberger et al., 1991). RsFC measures from fMRI data may provide a more objective, non-invasive means to assess the integrity of spinal cord functional circuits (Barry et al., 2017; Stroman, 2009; Stroman et al., 2004). Recent studies have demonstrated the potential of rsFC in spinal cord in case of diseases or after injury. Conrad et al. (2018) studied patients with multiple sclerosis who reported with focal lesions throughout the spinal cord. We have previously reported how unilateral injury to the dorsal column of the cervical spinal cord significantly weakened the strength of intra-segment horn-to-horn connectivity on the injury side and in slices below the lesion (Chen et al., 2015). The functional connectivity between ventral horn ROIs on neighboring segments below the lesion was also significantly weakened. However, that study did not perform a detailed investigation on how injury effected inter-spinal segment connectivity between all the functional regions, and looked mainly at acute post-injury effects rather than at different stages during recovery.

To summarize the goals of this study, we aimed (1) to extend our knowledge of the functional organization of the cervical spinal cord, and in particular to detect and characterize resting state networks beyond those reported in previous studies and (2) to demonstrate the functional relevance of measurements of resting state connectivity by quantifying plastic changes within spinal cord circuits during the process of recovery after SCI. We used a data-driven ICA technique to reveal functional networks within the spinal cord and measured connectivity within and between spinal segments. We also implemented a unilateral dorsal column lesion to observe any reorganization of spinal circuits post injury and at different stages of recovery. The results increase our understanding of the nature of intrinsic functional circuits within the cervical spinal cord and suggest how rsFC may be used as an imaging biomarker of the functional integrity of spinal cord.

2. Methods

2.1. Animal preparation

A total of 16 adult male squirrel monkeys (*Saimiri Sciureus*) were included in the study. Five of them underwent scans before and after unilateral dorsal column transections. Eleven other monkeys were scanned without injuries. During each MRI scan, the monkeys were anesthetized with isoflurane (0.8–1.2%) and mechanically ventilated, with head and body stabilized in a magnetic resonance (MR)compatible frame. Vital signals (cardiac and

respiratory cycles, core body temperature, end tidal CO2, SpO2 via pulse oximetry) were monitored and maintained within appropriate ranges throughout the imaging session. The respiration pattern during each fMRI scan was recorded and later used as a regressor in data preprocessing (see 2.4). The procedures were performed under a protocol approved by the Institutional Animal Care and Use Committee at Vanderbilt University. NIH and federal guidelines of the ethical use and care of research animals were followed.

2.2. Spinal cord injury: unilateral dorsal column lesion

Animals were under surgical level anesthesia (1.5–2% isoflurane) during aseptic surgery. The dorsal column was sectioned on the left-hand side (which had been established as the dominant hand using separate behavioral studies) with a fine pair of surgical scissors at the C5 level. The dura was then replaced with Gelfilm and covered with Gelfoam to protect the spinal cord. Muscle and skin were sutured during the enclosure. Monkeys were allowed to recover and carefully monitored. Monkeys received analgesics after each procedure. Further details of the surgical procedures can be found in our previous publications (Chen et al., 2012; Qi et al., 2011).

2.3. MRI data acquisition

MRI scans were acquired on an Agilent 9.4T scanner using a saddle-shaped transmit–receive surface coil (2.5 × 3 cm^2 in size) positioned over each animal's neck. Five contiguous axial image slices (each 3 mm in thickness) covering C3-C7 cervical segments, with the third slice positioned over the C5 segment (where the lesion was targeted), were acquired in each imaging session. Fig. 1 illustrates the locations of the five slices on sagittal and coronal imaging planes and the corresponding transverse axial images. High-resolution (0.25 × 0.25 mm^2 in-plane resolution, 128 × 128 matrix) structural magnetization transfer contrast (MTC) weighted images (TR (repetition time)/TE (echo time): 220/3.24 ms) were acquired using a gaussian radio frequency (RF) saturation pulse (flip angle, 820°; pulse width, 12 ms; RF offset, 5,000 Hz). FMRI imaging data were collected from the five contiguous slices covering C3-C7 segment. Each rsfMRI imaging run consisted of 300 dynamics acquired using a fast gradient echo sequence (flip angle ~18°, TR = 46.88 ms, TE: 6.5 ms, 3 s per volume) with an in-plane resolution of 0.5 × 0.5 mm^2 (64 × 64 matrix). For rsfMRI data acquisitions of the five animals which had pre- and post-injury data, a total of 14 runs were collected (3 runs each from 4 animals and 2 runs from 1 animal) at each of the four different imaging sessions: i) normal (or prelesion) condition, and at three timepoints post-SCI which were: ii) 2 weeks (post-SCI Stage1), iii) 7–8 weeks (post-SCI Stage2) and iv) 16–22 weeks (post-SCI Stage3). The choice of the timepoints was based on each animals' food reaching and grasping behaviors and in cage hand use after the injury. The most drastic behavioral impairment occurs within the first two weeks after injury. Impaired hand usage recovered significantly by seven to eight weeks. During 16–22 post-injury weeks, almost all monkeys had fully recovered hand use (Chen et al., 2015; Qi et al., 2013; Wang et al., 2018). Locations of the spinal nerve afferent bundles and their spatial relationships with the spinal cord were used as landmarks to align axial imaging plane across imaging sessions of the same animal and across animals. Data were acquired from the other eleven non-injured animals (31 runs in total) using the same protocol to illustrate the reproducibility of our results.

2.4. FMRI Data Preprocessing

All resting state fMRI data first underwent slice-by-slice 2D motion correction in MATLAB R2019a. Specifically, functional image volumes were first aligned using a 2D rigid body motion correction algorithm based on maximization of mutual information, with three motion parameters estimated (two translations and one rotation) slice by slice (Wu et al., 2019). Motion parameters (two translation and one rotation), along with temporal signals extracted from muscle and CSF regions containing at least 70% of the cumulative variance (derived using principal components analysis) were considered nuisance parameters and regressed out using a general linear model (Barry et al., 2018, 2017; Chen et al., 2015; Wu et al., 2019). No spatial smoothing was performed. The fMRI signals were then corrected for physiological noise (respiratory signal) using RETROICOR (Glover et al., 2000). Resting state fMRI signals were then band-pass filtered (Chebyshev type2 IIR filter, cut-off frequencies 0.01 and 0.1 Hz) prior to functional connectivity analyses. The axial fMRI images were up-sampled to 0.25 × 0.25 mm to match the anatomic images. A custom spinal cord structural MTC image template was generated based on pre-injury spinal cord MTC anatomic images from ten squirrel monkeys and used later in the analysis. Initially both pre- and post-lesion median fMRI images were co-registered to the structural MTC image in the individual subject space and the transformation was then applied to the fMRI time series data. In the second step each subject's anatomic images were co-registerd to the generated spinal cord template and the transformation was applied to the fMRI data using FSL to perform the group analysis (Jenkinson and Smith, 2001).

2.5. Independent Component Analysis (ICA) of resting state fMRI data

The co-registered functional data from the five injured monkeys were temporally concatenated to create a 2D Space × Concatenated Time data set and group ICA was performed on the resting state fMRI signals extracted from gray matter voxels segmented out using a manually drawn gray matter mask. Standard procedures in GIFT software (Calhoun et al., 2001) were followed and spatial ICA maps with their corresponding time series were obtained. Next, we used a dual regression technique to obtain subject-specific component maps, along with their associated time series (Beckmann et al., 2009). In spatial ICA, each component generally denotes a network which is spatially independent from other networks. For ICA decomposition, we chose 35 components from the 5 slices based on previous literature of spinal cord functional architecture and empirical evidences of synchronized BOLD fluctuations at specific regions, the details of which has been provided in Supplementary Method 1 along with figures (Supplementary Figures 1 & 2). The spatial component maps were thresholded (z-score > 3) and we classified them as dorsal and ventral horns, intermediate zones (extending from the intermediate part of spinal cord towards the dorsal region) and gray commissure (thin strip of gray matter located at the central junction between the two hemi-cords) region based on visual inspection of each component's spatial profile. We then considered the spatial location of each component as a ROI or functional hub for further evaluation, and calculated the functional connectivity between all such ROIs. Images from the eleven non-injury animals were similarly analyzed using ICA and the results are shown in Supplementary (Supplementary Fig 4) for comparison to the set of five animals which had images acquired before and after injury.

2.6. Functional Connectivity Measure and Power Spectra Analysis

Functional connectivity measures were derived at the individual subject as well as group level using the time series of each independent component (IC) (Joel et al., 2011). Between ROI connectivity (BROIC) was measured as the correlation between the time courses of pairs of independent components. Pearson's correlation coefficients (r values) were used to compute BROIC between all ROI pairs. The elements (r value) in the BROIC matrix for which $p < 0.05$ (FDR corrected) were considered as statistically significant. Those correlations which were significant within a slice or between neighboring slices, more than once, were considered reproducible connectivities. Whisker Box-plots of BROIC measures were obtained at different time points i.e. pre-SCI and post-SCI Stage1,2&3. Different groups were compared using Wilcoxon non-parametric tests and significant differences ($p < 0.05$ & $p < 0.01$) were noted.

We also evaluated group differences in power spectra. Power Spectra of the time course of each IC was computed and analyzed separately in three bands i.e., a) 0.01–0.033 Hz, b) 0.033–0.066 Hz and c) 0.066–0.1 Hz (in addition to the entire power spectrum) in order to identify the frequency range that was most sensitive to spinal cord injury and that was used for further analysis. Whisker-boxplots of spectral power measures representing the distributions of the mean values of all the independent components at each frequency band as well as the entire spectrum were computed from all the monkeys at different time points. Different groups were compared using Wilcoxon non-parametric tests and significant differences ($p < 0.05$ & $p < 0.01$) were noted.

2.7. Network Analysis using Graph Theory

There have been limited number of studies which used graph-theory for evaluating the organization of the functional networks in the cervical spinal cord (Liu et al., 2016). The connectivity matrix (BROIC) formed from the correlation values between each ROI pair was thresholded to retain only significant values ($p < 0.05$, FDR corrected). A simple network analysis was performed on the thresholded matrix using the 'Brain Connectivity Toolbox' based on graph theory principles (Rubinov and Sporns, 2010). In graph theory, a network is defined by a collection of nodes (vertices), and links (edges) between pairs of nodes. Nodes in our study represent the spinal cord ROIs (from all the slices), while links represent functional connectivity values between those ROIs. Next, the network was divided into different groups or communities based on the connectivity of nodes with each other (Newman, 2006). The optimal community structure is a subdivision of the network into non-overlapping groups of nodes in a way that maximizes the number of within-group edges and minimizes the number of between-group edges. These community structures provide a visual description of the functional network organization across the spinal cord. Finally, the original connectivity matrix (BROIC) was rearranged such that the ROIs from the same community are adjacent to each other, in order to illustrate the behavior of nodes within a community and between communities. This was done on data acquired before injury as well as at different stages after injury.

3. Results

3.1. Intrinsic functional organization identified by ICA analysis

ICA decomposes resting state fMRI data into seven spatially distinct components: Independent Component Analysis of rsfMRI data revealed the presence of seven components located at spatially distinct ROIs within a slice: left/right dorsal (LD&RD) horns, left/right ventral (LV&RV) horns, left/right intermediate (LI &RI) region which resides between the dorsal and ventral horns, and gray commissure (GC) region, which is the thin strip of gray matter that surrounds the central canal of the spinal cord, as shown by the spatial distribution of each independent component from a representative slice in Fig. 2 a. These ROIs were distinctly resolved spatially within the spinal gray matter, as illustrated in a 3D mesh plot in Fig. 2 b and Fig. 2 c where all the components from one slice are shown together. These ROIs represent clusters of voxels that show temporal synchrony in BOLD fluctuations independent of other clusters and may represent locally connected voxels and/or the spatial blurring effects of the intrinsic BOLD mechanism and imaging unsharpness (Shi et al., 2017). Supplementary Figure 3 presents a detailed description of the spatial location of the seven components from each of the five slices.

To show the specificity and robustness of the spatial distribution of the ICs, we performed a reproducibility test on data acquired from eleven healthy monkeys and compared the results to those obtained for the five monkeys that underwent both pre- and post-injury data acquisition. The close similarity in the spatial locations of the independent components between the five and eleven-monkey data is visually evident in Supplementary Figure 4. A quantitative analysis using Dice scores from one slice revealed a similarity of 1 for LD,0.97 for RD, 1 for LV, 0.7 for RV,0.94 for LI,0.98 for RI and 0.78 for GC. The remaining analyses in this study include only the pre- and post-injury data from the five injury-model monkeys.

Pair-wise correlations between ROIs reveal significant intra-and neighboring inter-slice connectivity: Fig. 3 a shows the matrix of correlation values between pairs of ROIs derived from ICA with significant correlations ($p < 0.05$) after FDR correction being denoted by *.Correlation matrix is obtained by averaging over the control (pre-lesion) group monkey data (14 runs). There were ten intra-slice connectivities which were significant ($p < 0.05$, FDR corrected) out of which six were observed in more than one slice (dorsal-dorsal, left ventral-left intermediate, right ventral-right intermediate, left ventral- gray commissure, right ventral-gray commissure and left intermediate-gray commissure), the details of which are shown in Supplementary Table 1. We also identified twelve neighboring inter-slice connectivities which were significant ($p < 0.05$, FDR corrected) out of which five were observed in more than one neighboring slice combination (right dorsal-right dorsal, left dorsal-left dorsal, right dorsal-left dorsal, left dorsal-right dorsal, left ventral-left ventral). Those significant intra-slice and neighboring inter-slice ROI pairs which were observed in more than one slice were considered reproducible ROI pairs. Details of the significant intra-slice and neighboring inter-slice ROI pairs are provided in Supplementary Table 1 with the reproducible ROI pairs highlighted.

Left dominant hand sided ROI pairs show stronger connectivity: Within a slice, the LD-RD pair has the highest absolute mean correlation coefficient averaged over all slices, whereas between neighboring slices, LD-LD has the highest absolute mean correlation value (Figure 3 b&c). Within a slice, the absolute mean correlation coefficient of all the left-sided ROI pairs was higher than their corresponding right-sided pairs with LV-GC and LI-GC having significantly higher correlations ($p < 0.01$) than their corresponding right side counterparts RV-GC and RI-GC (Fig. 3b); and in the case of neighboring slice ROI pairs, the mean correlation coefficient of all the left-sided ROI pairs were higher than their corresponding right-sided pairs, with LV-LV, LI-LI and GC-LV pairs having significantly higher correlations ($p < 0.01$) than their corresponding right sided ROI pairs RV-RV, RI-RI and GC-RV (Fig. 3 c). Figure 3 d&e summarizes the comparison between left and right sided connectivities for intra-slice and neighboring slice respectively using a schematic. All animals included in this study were left-handed, which indicates that the spinal gray matter subdivisions on the dominant left-hand side have stronger intrinsic connections within each segment and across segments.

3.2. Change in functional connectivity strength at different time points after SCI

Differential effects of SCI on intra-slice and neighboring inter-slice connectivity: Fig. 4 a shows the connectivity matrix of correlation values at different time points pre- and post-SCI (Stage1, Stage2 and Stage3). Intra-slice values are highlighted by black triangles and neighboring inter-slice connectivities are highlighted by black squares. The lesion produced by the injury was located at C5 (Slice 3) level. Box-plots for intra-slice (Fig. 4b) and neighboring slice connectivities (Fig. 4c) are computed from all the constituent ROI pairs of the respective segment or neighboring segments respectively. The intra-slice connectivity was significantly weakened post-SCI at Stage1&2 for Slice2/C6, which is below the lesion. Conversely, for above-lesion slices (Slice4/C4 and Slice5/C3), connectivity appeared to be significantly strengthened after injury and increased with time.

The inter-segmental connectivities between neighboring segments/slices dropped significantly both below and above the injury site at Stage1 post-SCI, as shown in Fig. 4c. There was a gradual increase in neighboring segment connectivity over time after injury (at Stage2 and Stage3) with majority of them either recovering back to pre-lesion normal level (Slice2-Slice3/C5-C6 and Slice3-Slice4/C4-C5) or even sur-passing pre-lesion connectivity (Slice4-Slice5/C3-C4) by the last time point except Slice1-Slice2/C6-C7 which remained significantly below baseline.

Differential effects of SCI on the reproducible ROI pairs: The reproducible ROI pairs within a slice (Supplementary Figure 5) and between neighboring slices (Supplementary Figure 6) were also studied individually and results are noted in Supplementary Result 3. It was found that two intra-slice ROI pairs (LD-RD at both above and below lesion and GC-LV at below the lesion) had significant decreases in connectivity post-injury, whereas for neighboring inter-slice ROI pairs, all the five ROI pairs had significant decreases in connectivity both above and below the lesion (except RD-LD above lesion).

3.3. Graph Theory based network analysis revealed changes in network community structures after SCI

Graph Theory was used to construct putative functional networks involving ROIs that shared connectivity patterns and it identified distinct ROI communities across the spinal segments in normal and post injury spinal cord. Fig. 5 a shows the connectivity matrix at different time points re-arranged to separate each of these groupings or communities. In normal cord (Pre-SCI) there are two dominant communities as shown by 1 st column in Fig. 5b: i) dorsal horns (RD and LD) from all the segments shown in yellow (named as 2 nd Community) and ii) the rest of the ROIs from ventral horns, intermediate zone and gray commissure region from several slices/segments (RV, LV, RI, LI and GC from all slices except RV of Slice3/C5 and RI of Slices1&3 (C7&C5) shown in red (named as 1 st community). Supplementary Results 4 along with Supplementary Figure 7 describes graph-theory network and community structure formation in details. A section of the left dorsal column tract at C5 segment (Slice3) disrupted these community structures and the pattern of strong connections between inter-segments was altered. Instead, intra-segment ROIs exhibited stronger connections forming new communities. This is evident from Fig. 5b second column (Stage1 post-injury), where different communities are formed at different slices/segments. Here the communities reorganize and get limited to ROIs within each segment, so each of four slices (Slice 1,3,4&5) / (C3, C4, C5 & C7) forms a separate community. The ROIs from same community has the same color in the figure.

This pattern remains similar at post-SCI Stage2. At Stage3 the inter-segment community structure starts to recover and the analysis groups all the ROIs within Slices4&5/C3&C4 (red colored) distinct from all ROIs across Slices1,2&3/C5,C6&C7 (yellow colored).

After noting the community reorganization due to injury in Fig. 5, we next quantified how the strength of the two major communities of the normal spinal cord underwent plastic changes after injury. Fig. 6 shows that intra-community strength of the two major communities of normal spinal cord underwent significant changes after the injury. Intra-community strength comprised the strength of each of the node or functional hub within that community. Node strength is calculated as the sum of weights of all the links (within a community) connected to that node. Fig. 6c box plots shows that the intra-community strength of the 1st community is reduced significantly after injury although it recovers back to baseline strength by Stage2 post injury and shows significant recovery in strength at each post-injury stage. The strength of the 2nd community is reduced even more after injury. It increases in strength at each stage post-injury, but still remains significantly below baseline at the last time point.

3.4. Frequency domain analysis revealed drop in power post-SCI predominantly in the 0.01–0.033 Hz frequency band

We also examined how the spectral amplitudes of IC time series were altered by SCI. The frequency spectra of all the independent components followed a similar pattern to each other as shown in Fig. 7a. The power spectra reached a peak value at approximately 0.01 Hz for all components. Reductions in power were observed post-injury, with the predominant decrease in power occurring in the first frequency band (0.01–0.033 Hz) as visible in the

shaded region in Fig. 7b. This observation was quantitatively substantiated through boxplots in c which shows that the decrease in power post injury was significantly higher in the 1st band than the other two frequency bands as well as the entire spectra, so this band was chosen for further analysis. Box plots in Fig. 7d show that post-SCI, there was a significant increase in power at Stage2 and Stage3 for the selected frequency band (0.01–0.033 Hz), though it remained significantly lower than baseline till the last time point at Stage3.

4. Discussion and Conclusion

We identified intrinsic networks in the gray matter of the spinal cord of non-human primates using resting state BOLD fMRI signals, and found patterns of connectivity that extend those found in previous studies. We also show these networks have functional relevance by documenting how intra- and neighboring inter-segmental connectivity changed over time after a unilateral dorsal column lesion at the C5 level. The current study extends the application of data driven ICA that was previously used to assess human spinal cord (Kong et al., 2014) and quantified both within and between segment connectivities and how they change after an injury in a nonhuman primate model.

4.1. Refined intrinsic functional networks within cervical spinal segments

Seven functional hubs characterized by highly synchronized fMRI signal fluctuations were observed within segments of spinal cord gray matter using ICA. These seven functional hubs correspond well with the known laminae structures established from cellular subtypes and anatomical connectivity analysis (Diaz and Morales, 2016). Our previous observations of high correspondence between resting state fMRI signals and local field potentials within the spinal gray matter led us to believe that these subregions represent localized fine-scale intrinsic networks (Wu et al., 2019). Our observations in this study extend previous models that were limited to functional hubs in bilateral dorsal and ventral horns and identified three newly found subdivisions, namely left intermediate and right intermediate zones, which reside between dorsal and ventral horns and the gray commissure region.

There have been limited functional imaging studies that have reported the existence of intermediate networks in spinal cord in animals in this study. (Wu et al., 2019). In a previous study we used electrophysiology and high field fMRI to study the spinal cord in primates and used the intermediate GM region as a reference region (Wu et al., 2019). Small ROIs were drawn from the dorsal toward the ventral horn passing through the intermediate region on one side of the spinal cord and a seed was selected at the dorsal horn. In over half of the observations it was found that correlations decreased monotonically from a high value to a low value at the level of the intermediate gray matter, and then increased as the ventral region was approached. This observation was also verified using electrophysiology which suggested the existence of three distinct subdivisions which were dorsal, intermediate and ventral region in spinal cord. However, in that study we did not investigate the correlations of intermediate GM as a seed region. In this study we also identified one independent component at the gray commissure (GC, lamina X). In three previous studies, there has been a fleeting reference to the GC as a possible functional subregion in spinal cord as found in our current study (Chen et al., 2015; Kong et al., 2014; Nateras et al., 2016). In our previous

seed-based rsfMRI connectivity study, there was some evidence suggesting connectivity between the dorsal and ventral horn of one segment with the GC region of the same segment (Figure 2 a in the paper) which was not discussed in the report (Chen et al., 2015). Similarly, in the human cervical spinal cord study which used the ICA approach, Kong et al reported one independent component (IC) having a central spatial profile corresponding to the GC region in our study, but interpreted it to be of 'no interest'(Kong et al., 2014). Nateras et al also reported the presence of rsFC hub in central spinal cord in humans (C1-C4) (Nateras et al., 2016) but did not investigate how it is connected with other regions.

The identification of a functional hub at the gray commissure is significant. The Commissural System exists along the neuro-axis in brain, brainstem and spinal cord, and is regarded as a key structure for transmitting information between two body sides and coordinating bilateral motor behavior (Maxwell and Soteropoulos, 2020). Studies of human subjects with Commissural System damage suggest that cervical Commissural System is engaged in sensorimotor behavior and possibly goal-directed motor behavior (Maxwell and Soteropoulos, 2020). In our study, we observed strong connections between GC to the left intermediate zones and bilateral ventral horns in the cervical spinal segments. The significant (FDR corrected, $p < 0.05$) and robust intra-slice correlation of GC with ventral region on both sides of gray matter in our study (Fig. 3b) corroborates with previously published immuno-histological study results which reported that commissural interneurons connect to bilateral ventral horns and may be responsible for ventral-ventral connectivity and coordinated motor behavior (Bannatyne et al., 2003; Wu et al., 2019). Our network analysis indicates that the intermediate network forms strong connection with the ventral and gray-commissure region. The intermediate zone in the cervical spinal cord in which an IC is located is engaged in many spinal functions. The C3-C7 segments are important in motor control and execution. For example, skilled hand movements depend on coordination of control signals by descending pathways, such as the corticospinal tract (CST), and proprioceptive afferents (PAs). An important locus for this coordination is the spinal cord intermediate zone (Chakrabarty and Martin, 2011). This region leads to interactions that likely serve as afferent gating and modulation of descending control signals during movement. After spinal cord injury, spared CST and PAs axon sprout and contribute to rewiring spinal circuit and affecting motor recovery (Jiang et al., 2016). A quantitative investigation of neurons in the intermediate zone after long-term amputation of the unilateral upper arm in man also support strong connections between intermediate zone and ventral horn (Suzuki et al., 1995).

In our previous study on squirrel monkey cervical spinal cord, we detected intra-slice dorsal-ventral connectivity using seed-based analyses (Chen et al., 2015; Wu et al., 2019). However, MRI studies of the human spinal cord, failed to detect this connection robustly (Barry et al., 2017; Eippert et al., 2017a). In the current study we did not observe strong dorsal-ventral connectivity, but strong intermediate-ventral correlations were observed on both sides of the spinal cord. The intermediate ROIs extended from the middle region (between dorsal and ventral horns) towards the dorsal region, and may overlap with the dorsal seed voxels used in previous seed-based analyses. This emphasizes the importance of standardizing the location of ROIs and defining voxels of each seed for comparison purposes

because they influence the interpretation of fMRI data analysis, as pointed out by others (Eippert et al., 2017a; Wu et al., 2019).

4.2. Neighboring Inter-segmental connectivities

Our results show that in addition to the intra-segmental connectivity between different functional hubs, there is strong inter-segmental connectivity across neighboring segments within C3-C7. Previous studies have reported the presence of correlations (including anti-correlations) between different spinal segments (Chen et al., 2015; Kong et al., 2014) but these were not studied in detail. The ventral ROIs of neighboring slices are unilaterally correlated across the segments whereas the dorsal ROIs are both unilaterally and bilaterally connected both within and across the segments (Supplementary Table1). Supplementary Table 1 shows that significant and reproducible dorsal connectivities exist both within a slice (LD-RD) and between neighboring slices (LD-LD, RD-RD, LD-RD and RD-LD) across C3-C7. Dorsal connectivities from all the segments further stood out as they formed a separate functional group before injury as shown by the graph-theory based community structure. The results also show that in the pre-injury correlation matrix (Figure 3a) there are strong correlations between ROIs of neighboring slices, with reduced connectivity between slices farther away from each other, which is a trend previously reported for monkey and human spinal cord (Chen et al., 2015; Kinany et al., 2020; Kong et al., 2014)

The results of graph-theory analysis separated connectivities of similar characteristics into communities, with higher intra-community connectivity and lower inter-community connectivity. The pre-lesion community structure suggested strong connections not only within a segment but also across multiple segments along the length of the spinal cord. A closer look at the community structure reveals that dorsal horns are highly connected to each other, forming a separate community, whereas the ventral, intermediate and GC regions remain inter-connected to each other, forming another community. These results indicate that while dorsal connectivity is bilateral but disjoint, bilateralism in ventral and intermediate ROIs occurs through an interaction with the GC junction, thus extending the ideas proposed previously by others (Kong et al., 2014; Wu et al., 2019). The results of community structure (Fig. 5) also suggest that bilateral functional hubs are grouped into same community representing strong connection between them.

4.3. Stronger intra- and neighboring inter-segmental functional connections on the dominant hand side

Overall, we found that many of the inter-ROI connectivities on the left hand (dominant hand) side were significantly stronger compared to their corresponding right sided ROI pairs as shown by the whisker boxplots in Fig. 3 b&c. The gray matter ROIs on the dominant left-hand side showed both strong intra-segmental and neighboring inter-segmental connections. To our knowledge, this is the first report of a stronger intrinsic functional connectivity associated with hand dominance in non-human primate cervical spinal cord. Previous studies have shown that resting-state networks can be dynamic, and they can be influenced by performing tasks (Cecchetto et al., 2019; Hasson et al., 2009; Muraskin et al., 2016). In this study, since the monkeys were left handed, they very likely performed majority of their daily routine tasks using their left hand (such as food reaching and grasping). This

may lead to stronger left-sided connectivity among the segments that control hand behavior. This hypothesis is aligned with our observations in the monkey somatosensory system, in which somatotopically matched digits regions that are involved in the same hand behavior exhibited strong rsFC and the pattern of rsFC aligned closely to the underlying anatomical connections (Wang et al., 2013). It could also suggest that neurons that work together during a task or behavior also wire together, and show synchronized fluctuation of BOLD signals at rest.

4.4. Differential effects of spinal cord injury on functional connectivity of within and between segments below and above the lesion

Both intra-segmental and neighboring inter-segmental ROI connectivity significantly weakened as a result of spinal cord injury as is evident from Fig. 4. However, neighboring inter-segmental connectivity was more affected by injury as seen by the significant weakening of the neighboring segment correlations, in contrast to the isolated decrease of intra-segment connectivity in Slice2/C6, which is one segment below the injury. Also, the connectivity between all five-reproducible neighboring inter-segment ROI pairs reduced significantly, whereas only two out of six reproducible intra-segment ROI pairs reduced significantly (Supplementary Figure 5 & 6). Thus, our results show that a unilateral section of the dorsal spinal cord disrupted the inter-segmental connectivity along the length of the spinal cord. However, intra-segmental functional connectivity gets damaged below the injured segment as previously observed by Chen et al (Chen et al., 2015).

Overall, there was a decrease in connectivity post-injury followed by a gradual increase over time as has been reported in literature before (Chen et al., 2015). Many of the intra-slice and neighboring inter-slice connectivities (Fig. 4), their reproducible ROI pairs (Supplementary Figure 5&6) showed significant increases ($p < 0.05$) with time. Most of them recovered back to pre-injury baseline levels by the last time point.

The within segment connectivity at Slice2/C6 segment which is just below the injury level weakened significantly after injury at Stage1 consistent with our previous observation (Chen et al., 2015) and returned to baseline at the last time point (Fig. 4 b). In contrast, injury strengthened the within segment connectivity of those above the lesion segment (C5) at C3/Slice5 and C4/Slice4. These connectivities even surpassed the baseline significantly at the end of recovery Stage3.

Between segment connectivity (Fig. 4 c) regardless of their functional group (C5-C6-C7, or C3-C4) weakened drastically during the post-injury Stage1, but recovered to prelesion level at Stage3 (except Slice1-Slice2/C6-C7). C6-C7/Slice1-Slice2 connectivity which is below the lesion, appeared to be the most affected due to injury, as they remained significantly lower than baseline until the last time point. In contrast, C3-C4/Slice4-Slice5 connectivity which is above the lesion surpassed the baseline significantly by the last time point. Thus, the two functional circuits below and above the lesion (C5-C6-C7 and C3-C4) underwent different plastic changes in connectivity (both within and between segments) after the injury. These changes likely reflect their roles in mediating or promoting recovery after injury.

Previous studies have provided evidence of recovery of damaged tissue to its pre-injury state after unilateral spinal cord lesion as a result of neuroplasticity (Qi et al., 2013; Reed et al., 2016). It has been reported that when the dorsal column injury is incomplete and spares some axons, surviving primary afferents and second-order spinal cord projections are able to project to the cuneate nucleus (Reed et al., 2016). The severity of the impairment and the capacity for recovery are directly correlated with the amount of axon terminals spared in the cuneate nucleus. Considerable behavioral recovery and cortical reorganization occurred even in the monkey with only 1% of axons spared in the dorsal column (Qi et al., 2013)

The power spectra analysis of the ICs (Fig. 7) also showed significant reduction of spectral power after SCI. The frequency band 0.01–.033 Hz was conspicuous because maximum reduction in power occurred in this frequency range post SCI. Following the injury, the spectral power at Stage2 and Stage3 increased significantly ($p < 0.05$) with time signifying recovery.

4.5. Graph theory community structures reveal injury-induced reorganization of intra-and inter-segmental functional networks

The graph theory analyses (Fig. 5) illustrate how the networks of functional hubs rearrange and get dominated by intra-segmental connections after an injury. They also show that the functional organization within the spinal cord starts to recover back to its pre-lesion structure with time as inter-segmental connections recover. These alterations in functional networks illustrate the effects of network plasticity after injury. Before injury, gray matter ROIs formed strong functional networks within and across segments of spinal cord. After injury, the network structures reorganize by becoming confined to ROIs within each segment from being spread within and across segments before injury. This result suggests that predominantly inter-segmental networks are damaged due to injury, which is in accordance with box-plots of connectivity values that showed predominant drops in connectivity between neighboring inter-slices compared to intra-slice. The inter-segmental community starts reappearing by the last time point and this finding is also corroborated by box-plots results which found that neighboring inter-slice connectivity slowly recovers back to baseline with time. At this time point, C3-C4 segment grouped together to form a community whereas C5-C6-C7 formed another separate community. This plastic change appears to align well to the distinct functions of these two groups of cervical segments and underscores the functional relevance of spinal circuits identified by the fMRI.

Note that the community formed from dorsal horns seemed to be more affected as it stayed significantly below baseline strength until the last time point (Fig. 6) whereas the other major community formed of ventral, intermediate and gray commissure regions recovered back to baseline by Stage2. The significant damage of the dorsal horn community can be attributed to the fact that the spinal cord injury was inflicted at the dorsal column tract.

4.6. Limitations of the study

The animals of our study were anesthetized. It has been reported that anesthesia could influence the measurement of functional connectivity (Hutchison et al., 2014). However, we do not think the fine-scale intrinsic network and community structures revealed in this study

are a byproduct of anesthesia for three reasons. Firstly, we have previously observed high correspondence between connectivity measures of rsfMRI signals and local field potentials obtained under similar conditions (Wu et al., 2019). Secondly, we examined the changes in the functional connectivity patterns after injury under the same anesthesia condition rather than measurements at single times. Thirdly, while BOLD effects may be systematically reduced due to anesthesia, the patterns of connectivity between regions should not be affected.

5. Summary and Conclusion

In summary, this study found the presence of robust BOLD signal fluctuations located at the bilateral intermediate region and gray commissure regions of the spinal cord gray matter of squirrel monkeys, in addition to the dorsal and ventral horns. These regions form hubs that connect to each other in various patterns that may be identified using graph theory. Significantly stronger functional connections were observed between hubs on the dominant hand side both within and between segments. It was found that due to injury the neighboring inter-slice connectivity gets more affected than intra-slice connectivity. The effects of injury on neighboring inter-slice connectivity are evident along the length of the spinal cord both below and above the lesion region. These findings were also supported by changes in the community structures formed at different stages post-injury using graph-theory. The current study also observed that the BOLD signals of frequency band 0.01–0.033 Hz are most affected by injury. Finally, the results show that post injury connectivity measures increased gradually as animals recovered their function.

These results provide new insights into the spinal cord functional architecture of non-human primates, and characterizes changes in connectivity following an injury. Our results extend current understanding of the nature of functional circuits within the spinal cord and suggest that rsFC can be used to identify changes in the functional integrity of the spinal cord post an injury.

Supplementary Material

Refer to Web version on PubMed Central for supplementary material.

Acknowledgements

The study is supported by NIH grant NS092961 and DOD grant SC160154. The authors acknowledge Chaohui Tang, Yue Zou and Fuxue Xin for animal handling and scan assistance. The authors acknowledge Jamie Reed for proof reading of the manuscript and Reply to comments of the reviewers.

References

Alstermark B, Isa T, 2012. Circuits for skilled reaching and grasping. Annu. Rev. Neurosci 35, 559–578. doi: 10.1146/annurev-neuro-062111-150527. [PubMed: 22524789]

Bannatyne BA, Edgley SA, Hammar I, Jankowska E, Maxwell DJ, 2003. Networks of inhibitory and excitatory commissural interneurons mediating crossed reticulospinal actions. Eur. J. Neurosci 18, 2273–2284. doi: 10.1161/CIRCULATION-AHA.110.956839. [PubMed: 14622188]

Barry RL, Conrad BN, Smith SA, Gore JC, 2018. A practical protocol for measurements of spinal cord functional connectivity. Sci. Rep 8, 1–10. doi: 10.1038/s41598-018-34841-6. [PubMed: 29311619]

Barry RL, Rogers BP, Conrad BN, Smith SA, Gore JC, 2017. Reproducibility of resting state spinal cord networks in healthy volunteersvolunteers at 7 Tesla 31–40. 10.1016/j.neuroimage.2016.02.058.Reproducibility

Barry RL, Smith SA, Dula AN, Gore JC, 2014. Resting state functional connectivity in the human spinal cord. Elife 2014, 1–15. doi: 10.7554/eLife.02812.

Beckmann C, Mackay C, Filippini N, Smith S, 2009. Group comparison of resting-state FMRI data using multi-subject ICA and dual regression. Neuroimage 47, S148. doi: 10.1016/s1053-8119(09)71511-3.

Calhoun VD, Adali T, Pearlson GD, Pekar JJ, 2001. Group ICA of functional MRI data: separability, stationarity, and inference. Proc. ICA 2001, 155–160.

Cecchetto Cinzia, Fischmeister Florian Ph S, Reichert Johanna L, Bagga Deepika, Schöpf Veronika, 2019. When to collect resting-state data: The influence of odor on post-task resting-state connectivity. NeuroImage 191.

Chakrabarty Samit, Martin John, 2011. Postnatal refinement of proprioceptive afferents in the cat cervical spinal cord. European Journal of Neuroscience 33, 1656–1666.

Chen LM, Mishra A, Yang P-F, Wang F, Gore JC, 2015. Injury alters intrinsic functional connectivity within the primate spinal cord. Proc. Natl. Acad. Sci 112, 5991–5996. doi: 10.1073/pnas.1424106112. [PubMed: 25902510]

Chen LM, Qi HX, Kaas JH, 2012. Dynamic reorganization of digit representations in somatosensory cortex of nonhuman primates after spinal cord injury. J. Neurosci 32, 14649–14663. doi: 10.1523/JNEUROSCI.1841-12.2012. [PubMed: 23077051]

Conrad BN, Barry RL, Rogers BP, Maki S, Mishra A, Thukral S, Sriram S, Bhatia A, Pawate S, Gore JC, Smith SA, 2018. Multiple sclerosis lesions affect intrinsic functional connectivity of the spinal cord. Brain 141, 1650–1664. doi: 10.1093/brain/awy083. [PubMed: 29648581]

Diaz E, Morales H, 2016. Spinal cord anatomy and clinical syndromes. Semin. Ultrasound, CT MRI 37, 360–371. doi: 10.1053/j.sult.2016.05.002.

Eippert F, Kong Y, Brooks JC, Büchel C, Winkler AM, Andersson JL, Finsterbusch J, Tracey I, 2017a. Investigating resting-state functional connectivity in the cervical spinal cord at 3 T.. Neuroimage 147, 589–601. doi: 10.1016/j.neuroimage.2016.12.072. [PubMed: 28027960]

Eippert F, Kong Y, Jenkinson M, Tracey I, Brooks JCW, 2017b. Denoising spinal cord fMRI data: approaches to acquisition and analysis. Neuroimage 154, 255–266. doi: 10.1016/j.neuroimage.2016.09.065. [PubMed: 27693613]

Ferreira LK, Busatto GF, 2013. Resting-state functional connectivity in normal brain aging. Neurosci. Biobehav. Rev 37, 384–400. doi: 10.1016/j.neubiorev.2013.01.017. [PubMed: 23333262]

Glover GH, Li TQ, Ress D, 2000. Image-based method for retrospective correction of physiological motion effects in fMRI: RETROICOR. Magn. Reson. Med 44, 162–167 10.1002/1522-2594(200007)44:1<162::AID-MRM23>3.0.CO;2-E. [PubMed: 10893535]

Goldberger ME, Bregman BS, Vierck CJ, Brown M, 1991. Criteria for assessing recovery of function after spinal cord injury: behavioral methods. J. Neurotrauma 8, 3–9. doi: 10.1089/neu.1991.8.3.

Guerra-Carrillo B, MacKey AP, Bunge SA, 2014. Resting-state fMRI: a window into human brain plasticity. Neuroscientist 20, 522–533. doi: 10.1177/1073858414524442. [PubMed: 24561514]

Harel R, Asher I, Cohen O, Israel Z, Shalit U, Yanai Y, Zinger N, Prut Y, 2008. Computation in spinal circuitry: lessons from behaving primates. Behav. Brain Res 194, 119–128. doi: 10.1016/j.bbr.2008.07.013. [PubMed: 18687365]

Harrison OK, Guell X, Klein-Flugge MC, Barry RL, 2021. Structural and resting state functional connectivity beyond the cortex.. Neuroimage.

Hasson Uri, Nusbaum Howard C, Small Steven L, 2009. Task-dependent organization of brain regions active during rest. Proceedings of the National Academy of Sciences of the United States of America 106.

Hutchison RM, Hutchison M, Manning KY, Menon RS, Everling S, 2014. Isoflurane induces dose-dependent alterations in the cortical connectivity profiles and dynamic properties of the brain's functional architecture. Hum. Brain Mapp 35, 5754–5775. doi: 10.1002/hbm.22583. [PubMed: 25044934]

Isa T, 2019. Dexterous hand movements and their recovery after Central nervous system injury. Annu. Rev. Neurosci 42, 315–335. doi: 10.1146/annurev-neuro-070918-050436. [PubMed: 30939102]

Jenkinson M, Smith S, 2001. A global optimization method for robust affine registration of brain images. Med. Image Anal 5, 143–156. doi: 10.1016/S1361-8415(01)00036-6. [PubMed: 11516708]

Jiang Yu-Qiu, Zaaimi Boubker, Martin John H, 2016. Competition with Primary Sensory Afferents Drives Remodeling of Corticospinal Axons in Mature Spinal Motor Circuits. Journal of Neuroscience 36, 193–203. [PubMed: 26740661]

Joel SE, Caffo BS, Van Zijl PCM, Pekar JJ, 2011. On the relationship between seed-based and ICA-based measures of functional connectivity. Magn. Reson. Med 66, 644–657. doi: 10.1002/mrm.22818. [PubMed: 21394769]

Kinany N, Pirondini E, Micera S, Van De Ville D, 2020. Dynamic functional connectivity of resting-state spinal cord fMRI Reveals fine-grained intrinsic architecture. Neuron 108, 424–435. doi: 10.1016/j.neuron.2020.07.024, e4. [PubMed: 32910894]

Kong Y, Eippert F, Beckmann CF, Andersson J, Finsterbusch J, Büchel C, Tracey I, Brooks JCW, 2014. Intrinsically organized resting state networks in the human spinal cord. Proc. Natl. Acad. Sci. U. S. A 111, 18067–18072. doi: 10.1073/pnas.1414293111. [PubMed: 25472845]

Liu Xiaojia, Zhou Fuqing, Li Xiang, Qian Wenshu, Cui Jiaolong, Zhou Iris, Luk Keith, Wu Ed, Hu Yong, 2016. Organization of the intrinsic functional network in the cervical spinal cord: A resting state functional MRI study. Neuroscience 336, 30–38. [PubMed: 27590264]

Maxwell DJ, Soteropoulos DS, 2020. The mammalian spinal commissural system: properties and functions. J. Neurophysiol 123, 4–21. doi: 10.1152/jn.00347.2019. [PubMed: 31693445]

Muraskin Jordan, Dodhia Sonam, Lieberman Gregory, Garcia Javier O, Verstynen Timothy, Vettel Jean M, Sherwin Jason, Sajda Paul, 2016. Brain dynamics of post-task resting state are influenced by expertise: Insights from baseball players. Human Brain Mapping 37.

Nateras OSE, Yu F, Muir ER, Bazan C, Franklin CG, Li W, Li J, Lancaster JL, Duong TQ, 2016. Intrinsic resting-state functional connectivity in the human spinal cord at 3.0 T. Radiology 279, 262–268. doi: 10.1148/radiol.2015150768. [PubMed: 26505923]

Newman MEJ, 2006. Finding community structure in networks using the eigenvectors of matrices. Phys. Rev. E - Stat. Nonlinear, Soft Matter Phys 74, 1–19. doi: 10.1103/Phys-RevE.74.036104.

Prochazka A, Mushahwar VK, 2001. Spinal cord function and rehabilitation - an overview. J. Physiol 533, 3–4. doi: 10.1111/j.1469-7793.2001.0003b.x. [PubMed: 11351006]

Qi HX, Chen LM, Kaas JH, 2011. Reorganization of somatosensory cortical areas 3b and 1 after unilateral section of dorsal columns of the spinal cord in squirrel monkeys. J. Neurosci 31, 13662–13675. doi: 10.1523/JNEUROSCI.2366-11.2011. [PubMed: 21940457]

Qi HX, Gharbawie OA, Wynne KW, Kaas JH, 2013. Impairment and recovery of hand use after unilateral section of the dorsal columns of the spinal cord in squirrel monkeys. Behav. Brain Res 252, 363–376. doi: 10.1016/j.bbr.2013.05.058. [PubMed: 23747607]

Reed JL, Liao CC, Qi HX, Kaas JH, 2016. Plasticity and recovery after dorsal column spinal cord injury in nonhuman primates. J. Exp. Neurosci 2016, 11–21. doi: 10.4137/JEN.S40197.

Rossignol S, Frigon A, 2011. Recovery of locomotion after spinal cord injury: some facts and mechanisms. Annu. Rev. Neurosci 34, 413–440. doi: 10.1146/annurev-neuro-061010-113746. [PubMed: 21469957]

Rubinov M, Sporns O, 2010. Complex network measures of brain connectivity: uses and interpretations. Neuroimage 52, 1059–1069. doi: 10.1016/j.neuroimage.2009.10.003. [PubMed: 19819337]

Sher Y, Cohen O, Zinger N, Harel R, Rubinsky B, Prut Y, 2010. Spatiotemporal organization of neuronal activity in the cervical cord of behaving primates. Front. Neurosci 4, 1–10. doi: 10.3389/fnins.2010.00195. [PubMed: 20582256]

Shi Z, Wu R, Yang P-F, Wang F, Wu T-L, Mishra A, Chen LM, Gore JC, 2017. High spatial correspondence at a columnar level between activation and resting state fMRI signals and local field potentials. Proc. Natl. Acad. Sci 114, 5253–5258. doi: 10.1073/pnas.1620520114. [PubMed: 28461461]

Simpson LA, Eng JJ, Hsieh JTC, Wolfe DL, 2012. The health and life priorities of individuals with spinal cord injury: a systematic review. J. Neurotrauma 29, 1548–1555. doi: 10.1089/neu.2011.2226. [PubMed: 22320160]

Sprenger Christian, Finsterbusch Jürgen, Büchel Christian, 2015. Spinal cord-midbrain functional connectivity is related to perceived pain intensity: A combined spino-cortical fMRI study. Journal of Neuroscience 35.

Stroman PW, 2009. Spinal fMRI investigation of human spinal cord function over a range of innocuous thermal sensory stimuli and study-related emotional influences. Magn. Reson. Imaging 27, 1333–1346. doi: 10.1016/j.mri.2009.05.038. [PubMed: 19570637]

Stroman PW, Khan HS, Bosma RL, Cotoi AI, Leung R, Cadotte DW, Fehlings MG, 2016. Changes in pain processing in the spinal cord and Brainstem after spinal cord injury characterized by functional magnetic resonance imaging. J. Neurotrauma 33, 1450–1460. doi: 10.1089/neu.2015.4257. [PubMed: 26801315]

Stroman PW, Kornelsen J, Bergman A, Krause V, Ethans K, Malisza KL, Tomanek B, 2004. Noninvasive assessment of the injured human spinal cord by means of functional magnetic resonance imaging. Spinal Cord 42, 59–66. doi: 10.1038/sj.sc.3101559. [PubMed: 14765137]

Suzuki Hiroshi, Oyanagi Kiyomitsu, Takahashi Hitoshi, Ikuta Fusahiro, 1995. Evidence for transneuronal degeneration in the spinal cord in man: a quantitative investigation of neurons in the intermediate zone after long-term amputation of the unilateral upper arm. Acta Neuropathologica 89, 464–470. [PubMed: 7618445]

Van den Heuvel MP, Hulshoff Pol HE, 2010. Exploring the brain network: a review on resting-state fMRI functional connectivity. Eur. Neuropsychopharmacol 20, 519–534. doi: 10.1016/j.euroneuro.2010.03.008. [PubMed: 20471808]

Wang Zheng, Chen Li Min, Négyessy László, Friedman Robert M., Mishra Arabinda, Gore John C., Roe Anna W., 2013. The Relationship of Anatomical and Functional Connectivity to Resting-State Connectivity in Primate Somatosensory Cortex. Neuron 78, 1116–1126. [PubMed: 23791200]

Wang Feng, Wu Tung-Lin, Li Ke, Chen Li Min, Gore John C., 2019. Spatiotemporal trajectories of quantitative magnetization transfer measurements in injured spinal cord using simplified acquisitions. NeuroImage: Clinical 23.

Wang F, Zu Z, Wu R, Wu TL, Gore JC, Chen LM, 2018. MRI evaluation of regional and longitudinal changes in Z-spectra of injured spinal cord of monkeys. Magn. Reson. Med 79, 1070–1082. doi: 10.1002/mrm.26756. [PubMed: 28547862]

Weber Kenneth A., Sentis Amy I., Bernadel-Huey Olivia N., Chen Yufen, Wang Xue, Parrish Todd B., Mackey Sean, 2018. Thermal Stimulation Alters Cervical Spinal Cord Functional Connectivity in Humans. Neuroscience 369.

Wei P, Li J, Gao F, Ye D, Zhong Q, Liu S, 2010. Resting state networks in human cervical spinal cord observed with fMRI. Eur. J. Appl. Physiol 108, 265–271. doi: 10.1007/s00421-009-1205-4.

Wu Tung Lin, Wang Feng, Mishra Arabinda, Wilson George H., Byun Nellie, Chen Li Min, Gore John C., 2018. Resting-state functional connectivity in the rat cervical spinal cord at 9.4 T. Magnetic Resonance in Medicine 79 (5).

Wu TL, Yang PF, Wang F, Shi Z, Mishra A, Wu R, Chen LM, Gore JC, 2019. Intrinsic functional architecture of the non-human primate spinal cord derived from fMRI and electrophysiology. Nat. Commun 10, 1–10. doi: 10.1038/s41467-019-09485-3. [PubMed: 30602773]

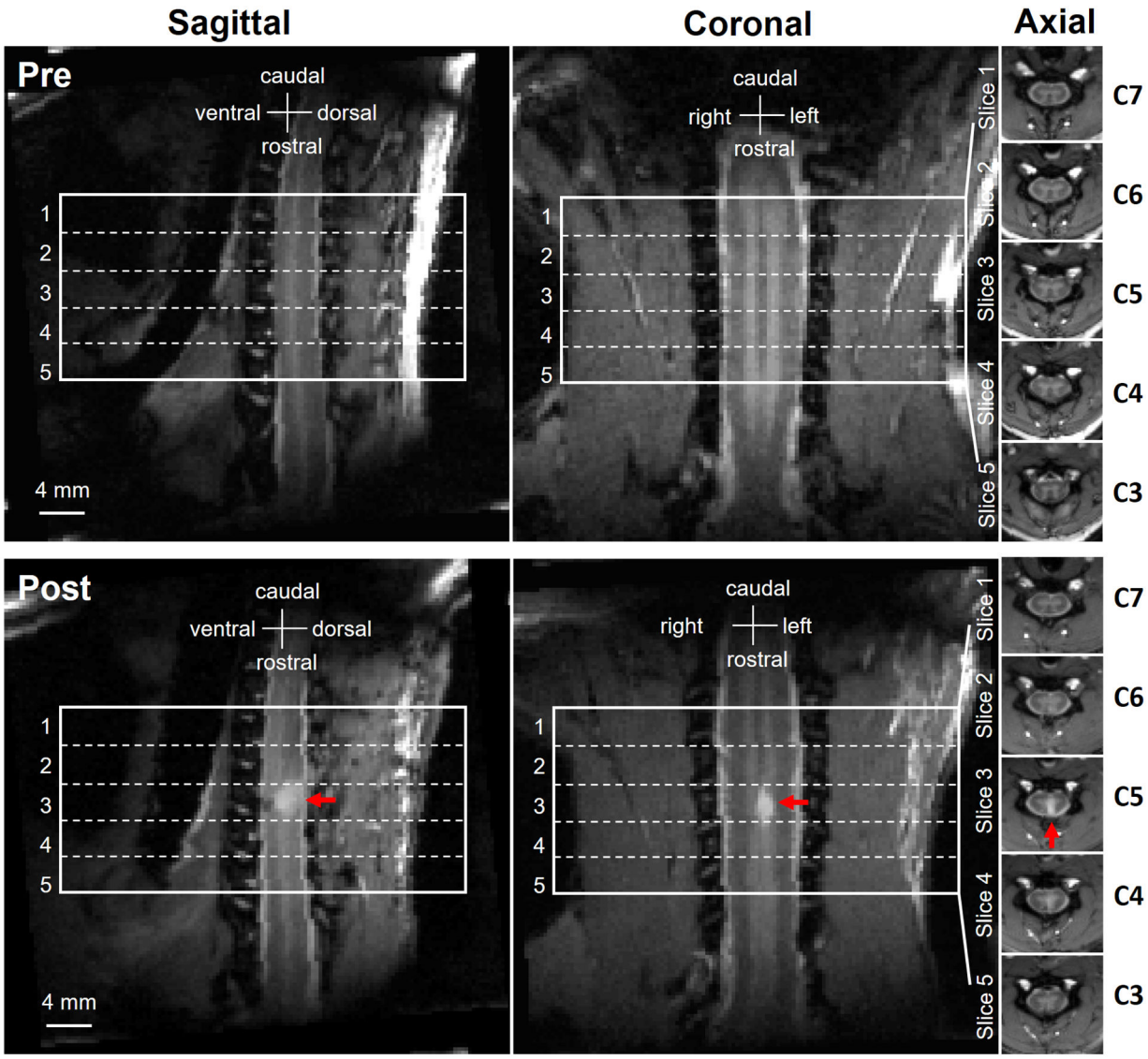

Fig. 1.

The locations of five axial slices on the sagittal and coronal planes obtained (a) pre- and (b) post-lesion in one representative monkey. The five axial slices correspond to C3-C7 cervical segments. The lesion site is on the middle slice (Slice3) corresponding to C5, indicated by red arrows.

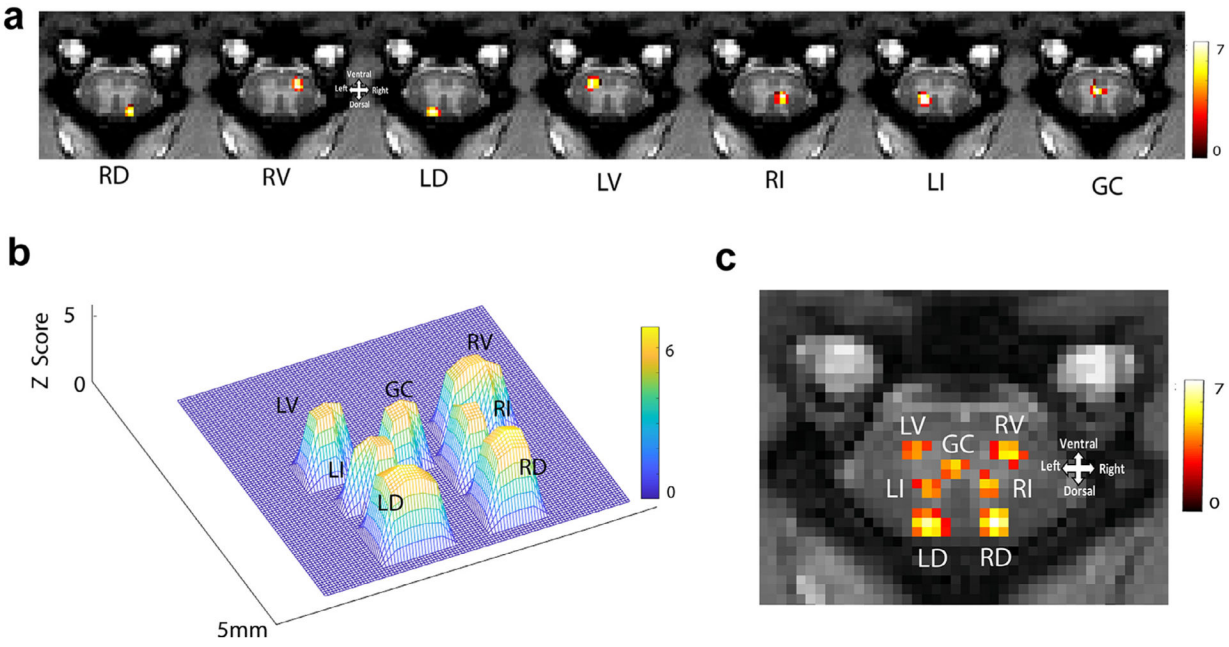

Fig. 2.

Spatial components derived from ICA representing regions of interest or functional hubs. (a) Spatial representation of seven independent component from a representative slice/segment (Slice5/C7). Each column represents the spatial distribution of one independent component. Coherent BOLD fluctuations localized at right dorsal (RD), right ventral (RV), left dorsal (LD), left ventral (LV), right intermediate (RI), left intermediate (LI) and gray commissure (GC) region are shown in the seven columns respectively. The color bar represents Z score which was thresholded at Z = 4. (b) 3D plot representing distinct spatial distribution of the seven components from a representative slice/segment (Slice5/C7) of spinal cord. (c) All the components from one slice/segment representing distinct spatial distribution of the functional hubs.

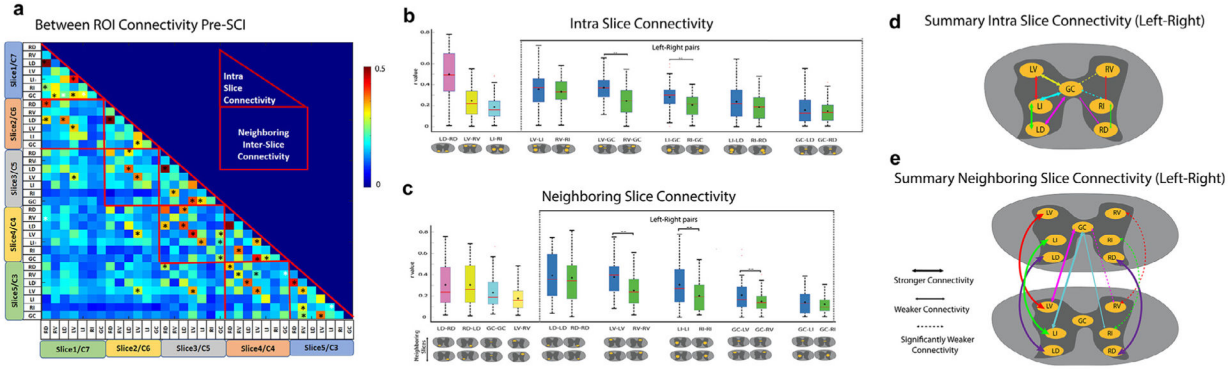

Fig. 3.

Intra-slice/segment and neighboring inter-slice/segment connectivity results of normal spinal cord and comparison between left and right sides. (a) Lower triangular correlation matrix obtained from all possible combinations of the ICs. Correlation Values (r) are thresholded between 0–0.5 range and significant correlations ($p < 0.05$) after FDR correction are denoted by *.Intra-slice and neighboring inter-slice connectivity are highlighted in red triangles and red squares respectively. All others are non-neighboring inter-slice connectivity. Correlation matrix is obtained by averaging over the control (pre-lesion) 5 monkey data (14 runs). The color bar represents r value. (b) Box plot presenting significant intra-slice connectivity (LD-RD, LV-RV, LI-RI, LV-LI, RV-RI, LV-GC, RV-GC, LI-GC, RI-RD, GC-LD) absolute values averaged over all slices. Corresponding non-significant connectivity (RI-GC, LI-LD, GC-RD) from contralateral side are also included for comparison. (c) Box plot of significant neighboring slice connectivity (LD-RD, RD-LD, GC-GC, LV-RV, LD-LD, RD-RD,LV-LV, RV-RV, LI-LI,GC-LV,GC-RV, GC-LI) absolute values averaged over all slices. Corresponding non-significant connectivity (RI-RI, GC-RI) from contralateral side is also included for comparison. Left-right connectivity pairs are shown within the dotted lines and are in blue and green box-plots respectively. Within the box-plots, the black diamond represent mean value and red line represent median value of the distribution. Significantly different ($p < 0.01$) left and right box-plots (Mann-Whitney U test) are denoted by **. Schematic view of the ROIs are shown below each box-plot. (d) and (e) show the summary comparison of the left and right side connectivity for intra-slice and neighboring inter-slice respectively. Each left sided connectivity and their corresponding right sided connectivity have the same color. Thinner arrow lines indicates weakened mean functional connectivity and dotted arrow lines indicate significantly weakened connectivity compared to the contralateral one.

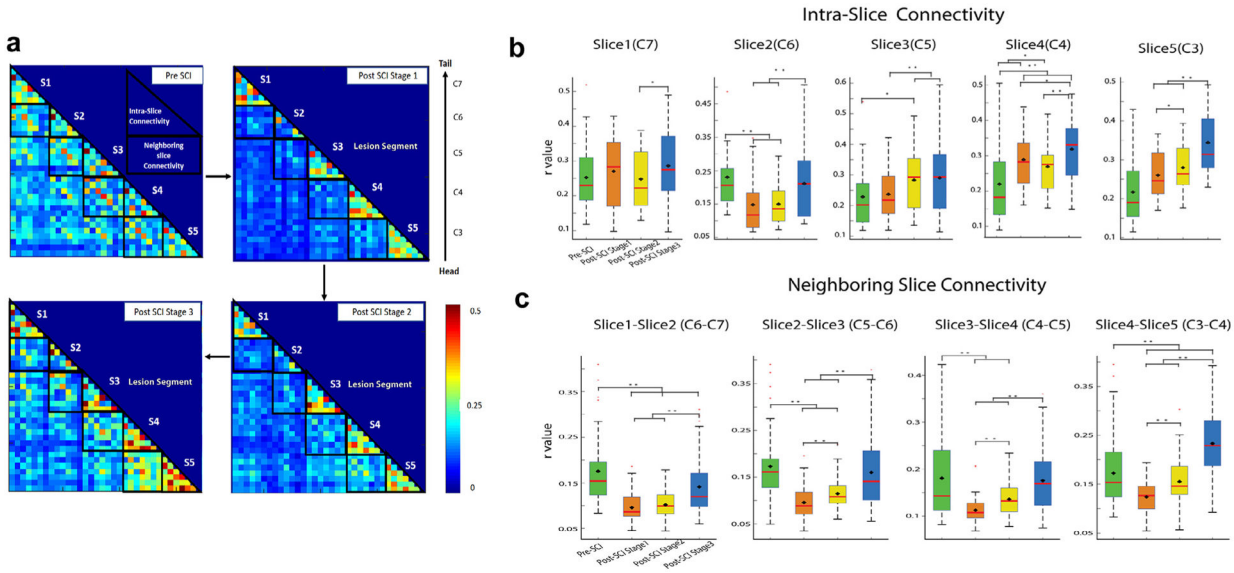

Fig. 4.

Intra- and neighboring inter-slice/segmental connectivity measures before and after injury at different time points. (a) Connectivity matrix of absolute correlation values of the IC pairs averaged over 14 runs of 5 monkeys at different time points (pre-SCI, post-SCI Stage1 (2 weeks), post-SCI Stage2 (7–8 weeks) and post-SCI Stage3 (16–22 weeks). Intra-slice and neighboring inter-slice connectivity is represented in black triangles and black box respectively. S1,S2,S3,S4 and S5 denotes the slice numbers which corresponds to spinal segments C7,C6,C5,C4 and C3 respectively. The lesion was at Slice3 (S3) correspondending to C5 segment. (b) Box-plot of intra-slice absolute connectivity measures at different time points for all the slices. (c) Box-plot of neighboring slice absolute connectivity measures at different time points for all the neighboring slice combinations. Box-plots for intra-slice and neighboring inter-slice connectivity is computed from all the constituent ROI pairs of the respective segment or neighboring segments. Within box-plots, the black diamond represent mean value and red line represent median value of the distribution. Significantly different box-plots (Wilcoxon non-parametric test) are denoted by *($p < 0.05$) and **($p < 0.01$).

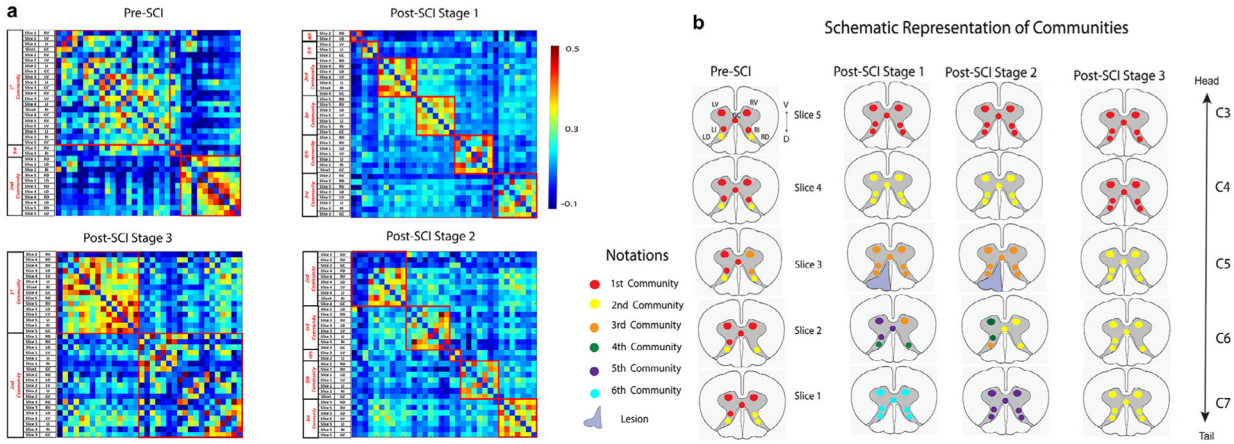

Fig. 5.

Graph Theory community analysis identifies reorganization of spinal cord functional circuits due to injury (Pre- and post-SCI Stage1, Stage2 and Stage3). (a) Connectivity matrix of all the ROIs from all slices arranged such that the nodes from same community are next to each other. The red boxes on the matrix highlight the communities formed and denote intra-community connectivity values. (b) Schematic diagram showing the resulting communities in different colors from graph-theory analysis at pre- and post-SCI at different time points. The rows represent the five slices/segments and each slice/segment contains the seven functional hubs or ROIs. The seven ROIs were right dorsal (RD), right ventral (RV), left dorsal (LD), left ventral (LV), right intermediate (RI), left intermediate (LI) and gray commissure (GC) region. No IR component was observed from Slice2/C6 and hence not shown. Data from 5 injury model-monkeys (14 runs each time-point) was included in this study.

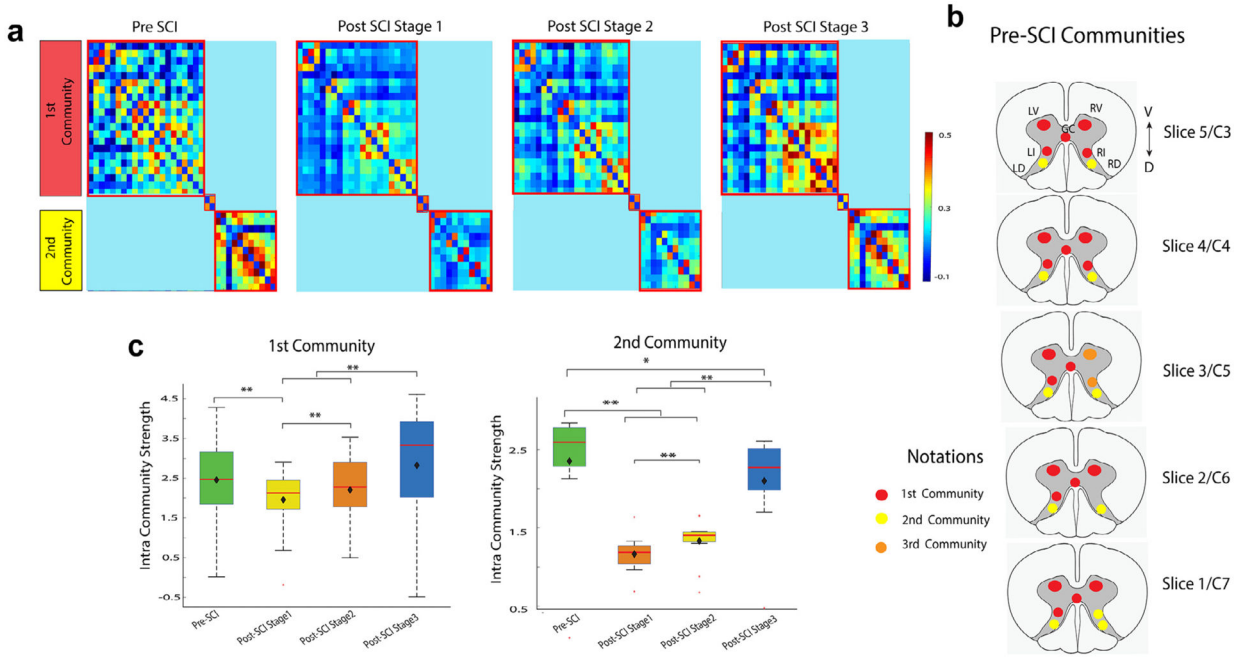

Fig. 6.

The major two spinal communities undergoes dynamic plastic change in community strength after injury. (a) Connectivity matrix at different time-points arranged according to pre-lesion community structure. The red boxes on the matrix highlight the pre-lesion communities. (b) Schematic diagram showing the community structure of the cervical spinal cord at pre-SCI as shown before in Fig. 5. (c) Box-plot comparison of intra-community strength at different stages for the 1st and 2nd Community. Within the box-plots, the black diamond represent mean value and red line represent median value of the distribution. Significantly different box-plots (Wilcoxon non-parametric test) are denoted by *($p < 0.05$) and **($p < 0.01$). Data from 5 injury model-monkeys (14 runs each time-point) were included in this study.

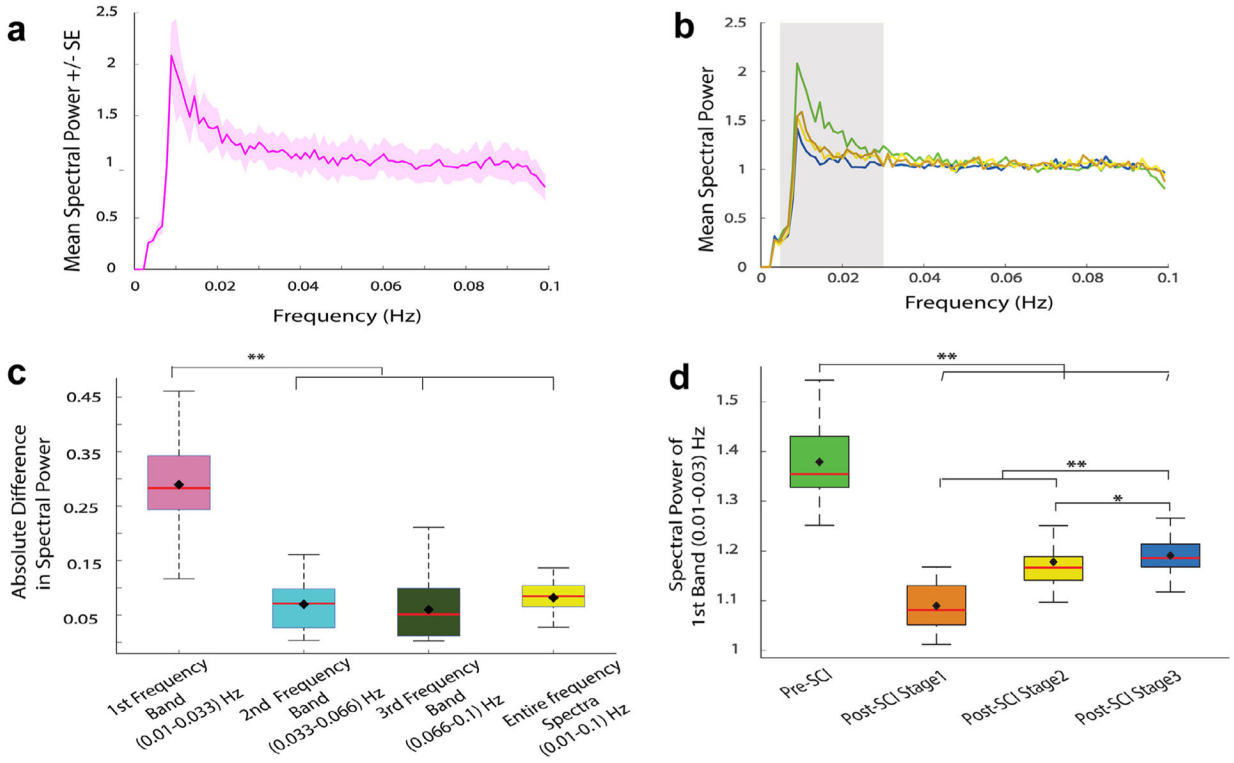

Fig. 7.

Effect of spinal cord injury on spectral power of independent components at different frequency bands. (a) Mean +/− SE(standard error) of all components pre-SCI. (b) Mean spectral power of all components at different stages i.e. pre- and post-SCI Stage1–3. Frequency range of interest (0.01–0.1 Hz) was divided into three bands i.e., i) 0.01–0.033 Hz, ii) 0.033–0.066 Hz and iii) 0.066–0.1 Hz. The shaded region indicates the 1st frequency band. (c) Box plot of absolute difference in spectral power between pre and post-SCI Stage1 for the three different frequency bands and entire spectra (0.01–0.1 Hz). (d) Box plot of spectral power at various stages of recovery for the 1st frequency band. Within the box-plots, the black diamond represent mean value and red line repressent median value of the distribution. Statistically significant difference using Wilcoxon non-parametric test are denoted by *($p < 0.05$) and **($p < 0.01$). Spectral Power analysis was averaged over all 5 injury model monkeys (14 runs) and all components at each time point.